

Article

Modeling and Control of Fluid Flow Networks with Application to a Nuclear-Solar Hybrid Plant

Zhe Dong * , Yifei Pan, Zuoyi Zhang, Yujie Dong and Xiaojin Huang

Institute of Nuclear and New Energy Technology, Collaborative Innovation Centre of Advanced Nuclear Energy Technology, Key Laboratory of Advanced Reactor Engineering and Safety of Ministry of Education, Tsinghua University, Beijing 100084, China; panyf15@mails.tsinghua.edu.cn (Y.P.); zyzhang@mail.tsinghua.edu.cn (Z.Z.); dongyj@mail.tsinghua.edu.cn (Y.D.); huangxj@mail.tsinghua.edu.cn (X.H.)

* Correspondence: dongzhe@mail.tsinghua.edu.cn; Tel.: +86-10-6279-6425

Received: 1 November 2017; Accepted: 18 November 2017; Published: 20 November 2017

Abstract: Fluid flow networks (FFNs) can be utilized to integrate multiple once-through heat supply system (OTHSS) modules based on either the same or different energy resources such as the renewable, nuclear and fossil for multi-modular and hybrid energy systems. Modeling and control is very important for the safe, stable and efficient operation of the FFNs, whose objective is to maintain both the flowrates and pressure-drops of the network branches within specific bounds. In this paper, a differential-algebraic nonlinear dynamic model for general FFNs with multiple pump branches is proposed based on both the branch hydraulics and network graph properties. Then, an adaptive decentralized FFN flowrate-pressure control law, which takes a proportional-integral (PI) form with saturation on the integral terms, is established. This newly-built control not only guarantees satisfactory closed-loop global stability but also has no need for the values of network hydraulic parameters. This adaptive control is then applied to the flowrate-pressure regulation of the secondary FFN of a two-modular nuclear-solar hybrid energy system and numerical simulation results show the feasibility and high performance of this network control strategy. Due to its concise form, this new flowrate-pressure FFN controller can be easily implemented practically.

Keywords: hybrid energy system; multi-modular energy system; fluid flow network; adaptive control

1. Introduction

Distributed energy systems can be built by electrical interconnection of power plants through the grid [1] and can also be built by thermal interconnection [2] of homogeneous or heterogeneous once-through heat supply system (OTHSS) modules based on fluid flow networks (FFNs). As shown in Figure 1, OTHSS refers to a thermodynamic system composed of a heat source, primary coolant circuit(s) and once-through steam generator(s) (OTSG) or once-through heat exchanger(s) (OTHX), whose heat source can be fired-coal, nuclear fission reaction, solar and etc. The coolant inside the primary circuits is used to absorb the heat from the source and transfers it to the secondary coolant through OTSGs or OTHXs. The secondary coolant is injected to the secondary side of the OTSGs or OTHXs and is changed to be the satisfactory working fluid for driving different thermal loads such as a steam turbine. Actually, OTHSS are very common in practical engineering such as the integral pressurized water reactors (iPWR, e.g., Nuscale, IRIS and mPower) with internal OTSGs [3–6], modular high temperature gas-cooled reactor (MHTGR, e.g., HTR-Module [7–9], MHTGR [10] and HTR-PM [11–13]) with side-by-side arranged OTSGs, concentrating solar power (CSP) plants with OTSGs [14] or OTHXs [15] and even coal-fired once-through boilers. A thermally interconnected distributed energy system is called a hybrid energy system (HES) [16–18] if the heat sources of OTHSS modules are of different types, otherwise it is called a multimodular energy system.

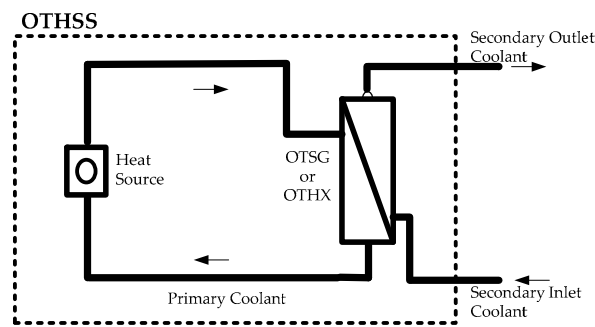


Figure 1. Schematic diagram of a once-through heat supply system (OTHSS) module.

FFNs can be used to build multimodular nuclear plants based on small modular reactor (SMRs) which are defined to be those fission reactors with electric power no more than 300 MW_e . Figure 2 illustrates the schematic diagram of a two-modular IRIS-based nuclear plant [19], where the live superheated steam flows of $331 \text{ }^\circ\text{C}/5.8 \text{ MPa}$ provided by the two IRIS-based nuclear steam supply system (NSSS) modules are combined together to drive the turbine and the condensed water are then pressurized by the feedwater pump and distributed to each IRIS module by the valves. The secondary-side of the fluid flow network (FFN) that interconnects these two IRIS modules of the plant is shown by Figure 3a, where branch f is the pump branch including the feedwater pump, branch i is the secondary side of the i th IRIS module ($i = 1, 2$) and branch 3 composes of the equipment such as the turbine, condenser, deaerator, etc. Similarly, m -modular IRIS plant can be realized by the parallel operation of m IRIS module through feedwater distribution and steam combination and the corresponding secondary FFN is illustrated by Figure 3b. Moreover, Figure 4 shows the simplified diagram of a two-modular MHTGR-based nuclear plant HTR-PM which is under construction at China, Shandong Shidao bay, where the NSSS module is mainly constituted by a pebble-bed MHTGR, a primary helium blower and a side-by-side arranged OTSG, each NSSS module is independently equipped with a feedwater pump and the live steam flows from multiple modules and with the parameters of $571 \text{ }^\circ\text{C}/13.9 \text{ MPa}$ are combined to drive the turbine [13]. The secondary FFN of HTR-PM plant is shown by Figure 5a and the FFN corresponding to the m -modular MHTGR plant with independent feedwater strategy is shown by Figure 5b [20]. From Figures 2–5, if the live steam parameters of different NSSS modules are identical, then these modules can be integrated by parallel operation, based on which the strong safety feature of SMRs can be applicable to large-scale nuclear plants at any desired power ratings.

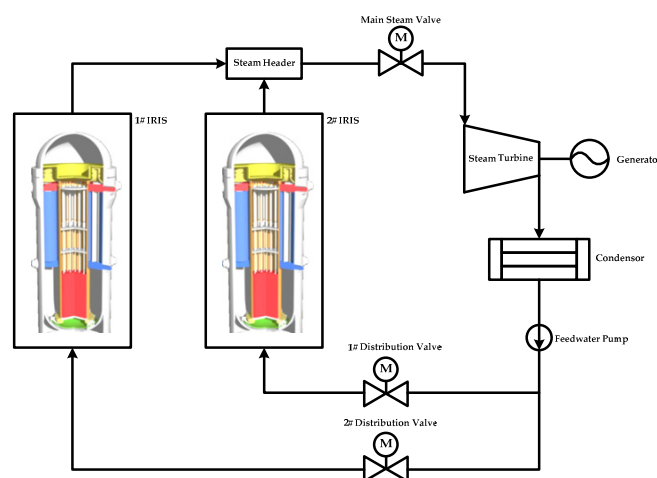


Figure 2. Schematic diagram of a two-modular international reactor innovative and secure (IRIS)-based plant.

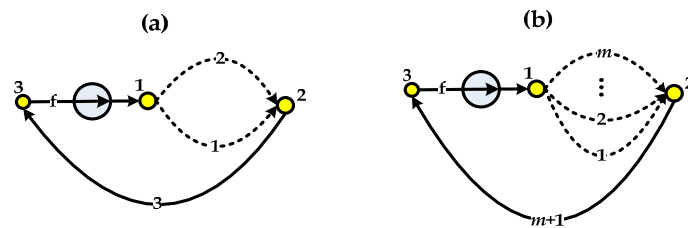


Figure 3. Secondary-side fluid flow network (FFN) of (a) 2 and (b) m modular IRIS plant by feedwater distribution.

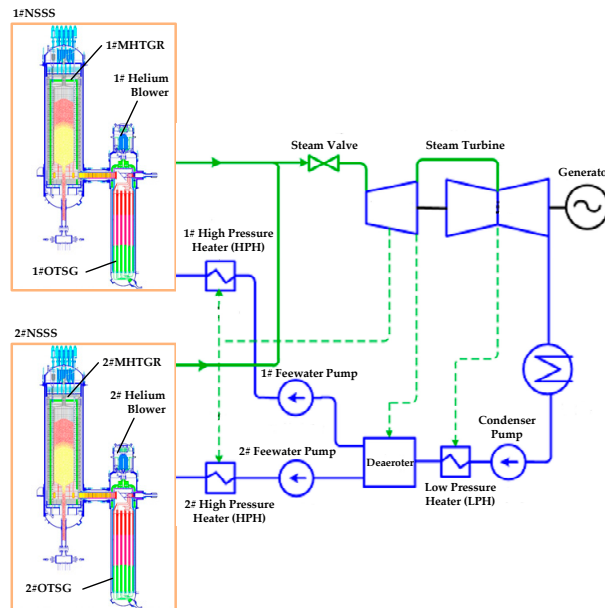


Figure 4. Schematic diagram of the high temperature reactor (HTR)-PM plant.

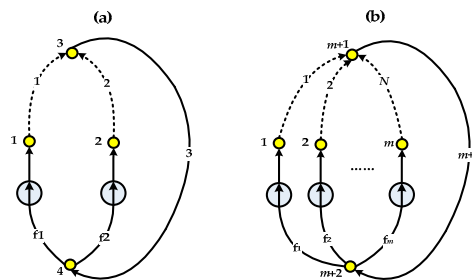


Figure 5. Secondary-side FFN of (a) 2 and (b) m modular high temperature gas-cooled reactor (MHTGR) plant by independent feedwater strategy.

Moreover, FFNs can also be applied to build nuclear-solar HESs by integrating the OTSSS modules based on NSSS and CSP. For CSP modules, the parabolic through collector (PTC) system and solar power tower (SPT) system are two significant types [21]. The PTC system consists of a group of reflectors that are curved in on dimension in parabolic shape to focus sunrays onto an absorber tube mounted in the focal line of the parabola. The SPT system uses a field of heliostats to reflect and concentrate the sunrays onto a central receiver placed in the top of a fixed tower. Both the PTC and SPT systems can power a secondary steam circuit and Rankine power cycle. Based on the secondary FFN given by Figure 3 or Figure 5, e.g., the SPT-based OTSSS proposed in [12] can be integrated in parallel with the MHTGR-based OTSSS introduced in [13] to realize a HES shown in Figure 6 if the live steam parameters of these heterogeneous OTSSS modules are identical. Furthermore, a nuclear-solar HES can also be realized by serial integration of different modules, e.g., Figure 7 gives the schematic

diagram of a serially integrated HES [13], where a PTC-based OTHSS is adopted to heat up the feedwater flow of a MHTGR-based NSSS module in parallel with a high-pressure heater (HPH). Here, in Figure 7b, branch f is the pump branch including the feedwater pump, branch 1 contains the original HPH, branch 2 is the secondary side of the PTC-based module, branch 3 is the secondary side of the OTSG of the MHTGR-based module and branch 4 composes of the equipment such as the turbine, condenser, deaerator and etc. Through the heterogeneous integration scheme shown by Figure 7, there is less necessity of storage devices with large capacity for the CSP-module, which leads to system simplification and cost reduction. Moreover, there is higher steam parameters, which induces better turbine efficiency. Therefore, based on the above introduction as well as the instances shown in Figures 2–7, FFN is central in thermally integrating homogeneous or heterogeneous OTHSS modules with parallel, serial and some other integration manners.

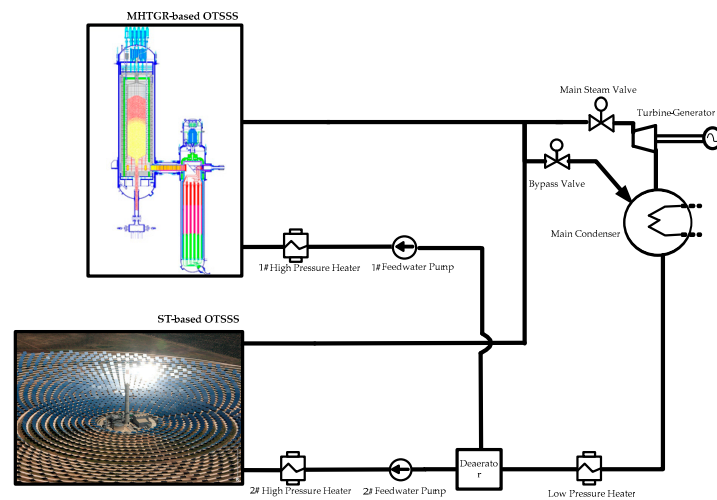


Figure 6. A nuclear-solar hybrid energy system (HES) constituted by an MHTGR-based and a solar power tower STP-based OTSSs.

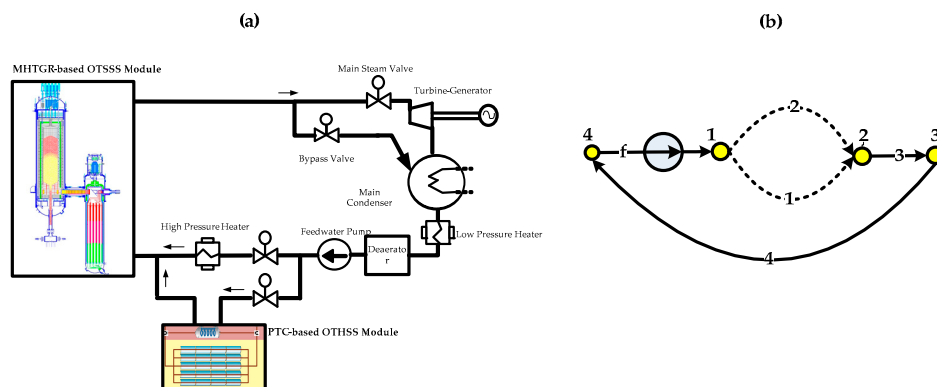


Figure 7. An HES constituted by an MHTGR-based OTSS module and a parabolic through collector (PTC)-based OTHSS module: (a) simplified process diagram; (b) structure of the FFN.

Based on the above discussion, to guarantee the stable and efficient operation of multi-modular or hybrid energy systems, it is basically needed to drive the flowrates and (or) pressure-drops of their secondary FFN to their desired values. To achieve this objective, it is crucial to give a proper FFN control law which is the mechanism of adjusting the resistances of network branches and (or) the pressure-heads of pumps or blowers by changing the valve openings and (or) the rotation speeds of pumps/blowers. FFN control method was studied since 1970s [22–25]. In [25], a FFN flowrate controller was proposed by Kocić based on the linearized model of a mine ventilation network, which however cannot handle the network nonlinearity. After 2000, some important progresses in

FFN control have been made [26–28]. By incorporating the branch fluid dynamics and network graph features, the non-minimal and minimal models for FFNs with single pump were proposed and two centralized flowrate controllers, which need the flowrate measurements of all the network branches, were also given [26]. By analyzing the dissipativity of FFN with a single pump, Dong proposed a decentralized flowrate controller that not only guarantees globally asymptotic stability (GAS) but also takes the simple proportional-integral (PI) form [27]. By giving a nonlinear differential-algebraic model for FFN with a single pump, a flowrate-pressure controller providing globally bounded stability was proposed in [28] and was then applied for realizing module coordination control of multi-modular nuclear plants integrated by the feedwater distribution scheme shown in Figure 3.

However, there is still no result in the dynamic modelling and flowrate-pressure control of general FFNs with multiple pumps or blowers, which is crucial in building multi-modular and hybrid energy systems based on integrating multiple OTHSS modules. In this paper, a nonlinear differential-algebraic model for FFNs with multiple pumps is proposed based on the branch dynamics and network graph property. Then, a novel adaptive decentralized flowrate-pressure controller is given for FFNs with a simple form. Finally, this newly-built control law is applied to realize the flowrate-pressure regulation for a FFN utilized to realize a two-modular nuclear-solar hybrid energy system (HES) and numerical simulation results show the feasibility and satisfactory performance of this newly-built FFN control. The novelty of this paper lies on two aspects, where the first one is to convert the control problem of hybrid and multimodular energy system to the control problem of FFNs and the second one is the modeling and flowrate-pressure control design for fluid flow networks.

2. Nonlinear Differential-Algebraic Model

Suppose that there are n branches without pump, m fan branches and n_c nodes in a FFN, where each fan branch has a single fan or pump. In this section, the branch dynamics and graph properties of a FFN are introduced and then a differential-algebraic model describing the FFN dynamics is given.

2.1. Branch Dynamics

Based on the conservation law of momentum, the fluid motion in the branches without pump can be written as [29]:

$$\dot{\mathbf{Q}} + \mathbf{K}\mathbf{Q}_D^2\mathbf{R} = \mathbf{KH} \quad (1)$$

where $\dot{\mathbf{Q}} = [Q_1, \dots, Q_n]^T$, $\mathbf{Q}_D^2 = \text{diag}(Q_1 | Q_1 |, \dots, Q_n | Q_n |)$, $\mathbf{K} = \text{diag}(K_1, \dots, K_n)$, $\mathbf{R} = [R_1, \dots, R_n]^T$, $\mathbf{H} = [H_1, \dots, H_n]^T$ and scalars Q_j , R_j , H_j and K_j is respectively the flowrate, dynamic resistance, pressure drop and inertia coefficient of branch j ($j = 1, \dots, n$).

2.2. Graph Properties

Assume that node i is connected to the fan branch i ($i = 1, \dots, m$). The fluid flow network can be divided in to a tree containing the fan branches and its complement, i.e., the co-tree whose branches are referred to as the links. The number of links is [30]:

$$l = (n + m) - (n_c - 1) = n + m + 1 - n_c \quad (2)$$

From Kirchhoff's voltage law (KVL) [30],

$$\begin{bmatrix} \mathbf{E}_H & \mathbf{O}_{(l-k) \times m} \\ \mathbf{e}_{Hf} & \mathbf{\Gamma}_{Hf} \end{bmatrix} \begin{bmatrix} \mathbf{H} \\ \mathbf{H}_f \end{bmatrix} = \mathbf{O} \quad (3)$$

where $\mathbf{H}_f = [H_{fj}]_{m \times 1}$, $\mathbf{E}_H = [E_{Hij}]_{(l-k) \times n}$, $\mathbf{e}_{Hf} = [e_{Hfij}]_{k \times n}$, $\mathbf{\Gamma}_{Hf} = [\lambda_{Hfij}]_{k \times m}$, k is the number of fundamental loops containing the fan branches, H_{fj} ($j = 1, \dots, m$) is the pressure drop of pump branch j . If branch j ($j = 1, \dots, n$) is contained in fundamental loop (FL) i ($i = 1, \dots, k$) with the same (opposite) direction, then $E_{Hij} = 1(-1)$, else $E_{Hij} = 0$. If branch j ($j = 1, \dots, n$) is in FL $l - k + i$ ($i = 1, \dots, k$) with the same

(opposite) direction, then $e_{Hfij} = 1(-1)$, else $e_{Hfij} = 0$. Moreover, if fan branch j ($j = 1, \dots, m$) is in FL $l - k + i$ with the same (opposite) direction, then $\lambda_{Hfij} = 1(-1)$, else $\lambda_{Hfij} = 0$. Here, H_f can be further expressed as

$$H_f = -H_d + R_f Q_f \tag{4}$$

where $H_d = [H_{dj}]_{m \times 1}$, $R_f = \text{diag}(R_{f1}, \dots, R_{fm})$, $Q_f = [Q_{fj}]_{m \times 1}$, H_{dj} is the pressure head provided by fan (or pump) j , Q_{fj} is the flowrate of pump branch j and R_{fj} is the resistance coefficient of pump branch j ($j = 1, \dots, m$).

From Kirchhoff's current law (KCL) [30],

$$\begin{bmatrix} E_Q & O \\ e_{Qf} & -\Gamma_{Qf} \end{bmatrix} \begin{bmatrix} Q \\ Q_f \end{bmatrix} = O \tag{5}$$

where $E_Q = [E_{Qij}]_{(n_c-m-1) \times n}$, $e_{Qf} = [e_{Qfij}]_{m \times n}$, $\Gamma_{Qf} = [\lambda_{Qfij}]_{m \times m}$. If branch j ($j = 1, \dots, n$) is connected to node $i + m$ ($i = 1, \dots, n_c - m - 1$) with flow going away (into) from node $i + m$, then $E_{Qij} = 1(-1)$, else $E_{Qij} = 0$. If branch j ($j = 1, \dots, n$) is connected to node $i + 1$ with flow going into node $i + m$, $E_{Qij} = 0$ if branch j is not connected to node $i + m$. If branch j is connected to node i ($i = 1, \dots, m$) with flow going into (away from) the node, then $e_{Qfij} = 1(-1)$, else $e_{Qfij} = 0$. If fan branch j is connected to node i ($i = 1, \dots, m$) with flow going into (away from) the node, $\lambda_{Qfij} = 1(-1)$, else $\lambda_{Qfij} = 0$.

2.3. Differential-Algebraic Network Model

It is not loss of generality to make the following assumptions:

- (A1) Branches 1 to l correspond to the links.
- (A2) Branches $l + 1$ to $n + m$ correspond to tree-branches and all the fan branches are in the tree.

From assumptions (A1) and (A2) as well as Equations (3) and (5),

$$\begin{bmatrix} E_{Hc} & E_{Ha} & O_{(l-m) \times m} \\ e_{Hfc} & e_{Hfa} & \Gamma_{Hf} \end{bmatrix} \begin{bmatrix} H_c \\ H_a \\ H_f \end{bmatrix} = O \tag{6}$$

$$\begin{bmatrix} E_{Qc} & E_{Qa} & O_{(n_c-m-1) \times m} \\ -e_{Qfc} & -e_{Qfa} & \Gamma_{Qf} \end{bmatrix} \begin{bmatrix} Q_c \\ Q_a \\ Q_f \end{bmatrix} = O \tag{7}$$

where $H_c = [H_1, \dots, H_l]^T$, $H_a = [H_{l+1}, \dots, H_n]^T$, $Q_c = [Q_1, \dots, Q_l]^T$, $Q_a = [Q_{l+1}, \dots, Q_n]^T$.

Then, based on the duality of KVL and KCL [30] and by choosing

$$\begin{bmatrix} E_{Hc} \\ e_{Hfc} \end{bmatrix} = I_l \tag{8}$$

$E_{Qa} = I_{n_c-m-1}$, $\Gamma_{Qf} = I_m$, $e_{Qfa} = O_{m \times (n_c-m-1)}$, i.e.,

$$\begin{bmatrix} E_{Qa} & O_{(n_c-m-1) \times m} \\ -e_{Qfa} & \Gamma_{Qf} \end{bmatrix} = I_{n_c-1} \tag{9}$$

we have

$$\begin{bmatrix} E_{Ha} & O_{(l-k) \times m} \\ e_{Hfa} & \Gamma_{Hf} \end{bmatrix} = - \begin{bmatrix} E_{Qc}^T & -e_{Qfc}^T \end{bmatrix} \tag{10}$$

From Equation (10),

$$\begin{bmatrix} E_{Ha} \\ e_{Hfa} \end{bmatrix} = -E_{Qc}^T \begin{bmatrix} E_{Ha}^T & e_{Ha}^T \end{bmatrix} \tag{11}$$

$$e_{Qfc} = \begin{bmatrix} O_{m \times (l-m)} & \Gamma_{Hf}^T \end{bmatrix} \tag{12}$$

From Equation (7),

$$Q_a = -E_{Qa}^{-1} E_{Qc} Q_c = -E_{Qc} Q_c \tag{13}$$

From Equations (3), (4), (8) and (11), we can derive that

$$H_c = - \begin{bmatrix} E_{Hc} \\ e_{Hfc} \end{bmatrix}^{-1} \left\{ \begin{bmatrix} E_{Ha} \\ e_{Hfa} \end{bmatrix} H_a - \begin{bmatrix} O_{(l-k) \times m} \\ \Gamma_{Hf} \end{bmatrix} (H_d - e_{Qf} R_f Q) \right\} = E_{Qc}^T H_a - S_{Qc} Q_c + S_d H_d \tag{14}$$

where

$$S_{Qc} = \begin{bmatrix} O_{(l-k) \times m} \\ \Gamma_{Hf} \end{bmatrix} R_f e_{Qfc} = e_{Qfc}^T R_f e_{Qfc} = \begin{bmatrix} O_{(l-m) \times (l-m)} & O_{(l-m) \times m} \\ O_{m \times (l-m)} & \Gamma_{Hf} R_f \Gamma_{Hf}^T \end{bmatrix} \tag{15}$$

$$S_d = \begin{bmatrix} O_{(l-m) \times m} \\ \Gamma_{Hf} \end{bmatrix} = e_{Qfc}^T \tag{16}$$

By substituting (14) with

$$K_c^{-1} \dot{Q}_c + Q_{cD}^2 R_c = H_c$$

we have

$$K_c^{-1} \dot{Q}_c = -S_{Qc} Q_c - Q_{cD}^2 R_c + E_{Qc}^T H_a + S_d H_d \tag{17}$$

Since E_Q is a constant matrix, from Equation (5),

$$E_Q \dot{Q} = O \tag{18}$$

Substitute (1) to (17),

$$E_{Qc} K_c H_c + E_{Qa} K_a H_a = E_{Qc} K_c Q_{cD}^2 R_c + E_{Qa} K_a Q_{aD}^2 R_a \tag{19}$$

Then from (14) and (19), we can obtain that

$$\left(E_{Qc} K_c E_{Qc}^T + K_a \right) H_a = E_{Qc} K_c \left(Q_{cD}^2 R_c + S_{Qc} Q_c - S_d H_d \right) + K_a Q_{aD}^2 R_a \tag{20}$$

The above analysis and derivation can be summarized as following Proposition 1.

Proposition 1. *The dynamics of fluid flow networks with multiple pumps can be expressed by differential-algebraic model*

$$\begin{cases} K_c^{-1} \dot{Q}_c = -S_{Qc} Q_c - Q_{cD}^2 R_c + E_{Qc}^T H_a + S_d H_d, \\ \left(E_{Qc} K_c E_{Qc}^T + K_a \right) H_a = E_{Qc} K_c \left(Q_{cD}^2 R_c + S_{Qc} Q_c - S_d H_d \right) + K_a Q_{aD}^2 R_a, \end{cases} \tag{21}$$

Remark 1. *From model (21), FFN dynamical behavior is given by branch hydraulic parameters R_{fj} ($j = 1, \dots, m$) and K_i ($i = 1, \dots, n$) as well as network topological matrices E_{Qc} and e_{Qfc} .*

3. Flowrate-Pressure Control Design

3.1. State-Space Model

Define

$$\mathbf{R}_c = \begin{bmatrix} \mathbf{R}_{cc}^T & \mathbf{R}_{cd}^T \end{bmatrix}^T = \begin{bmatrix} [R_{c1}, \dots, R_{c(l-m)}] & [R_{c(l-m+1)}, \dots, R_{cl}] \end{bmatrix}^T \quad (22)$$

$$\mathbf{S}_c = \begin{bmatrix} \mathbf{I}_{l-m} & \mathbf{O}_{(l-m) \times m} \end{bmatrix}^T \quad (23)$$

From Equations (16), (22) and (23),

$$\mathbf{R}_c = \mathbf{S}_c \mathbf{R}_{cc} + \mathbf{S}_d \mathbf{R}_{cd} \quad (24)$$

Suppose the referenced values (setpoints) of \mathbf{Q}_c , \mathbf{Q}_a , \mathbf{R}_{cc} , \mathbf{R}_a and \mathbf{H}_d are constant vectors \mathbf{Q}_{cr} , \mathbf{Q}_{ar} , \mathbf{R}_{crr} , \mathbf{R}_{ar} and \mathbf{H}_{dr} respectively. Define $\mathbf{Q}_{ce} = \mathbf{Q}_c - \mathbf{Q}_{cr}$, $\mathbf{Q}_{ae} = \mathbf{Q}_a - \mathbf{Q}_{ar}$, $\mathbf{R}_{cce} = \mathbf{R}_{cc} - \mathbf{R}_{crr}$, $\mathbf{R}_{ae} = \mathbf{R}_a - \mathbf{R}_{ar}$, $\mathbf{H}_{de} = \mathbf{H}_d - \mathbf{H}_{dr}$, where it can be seen from (13) that $\mathbf{Q}_{ae} = -E_{Qc} \mathbf{Q}_{ce}$. Here, \mathbf{R}_{cc} , \mathbf{R}_a and \mathbf{H}_d are chosen as the control input to regulate the branch flowrates and pressure-drops.

Then, the state-space model for control design can be expressed as

$$\begin{cases} \mathbf{K}_c^{-1} \dot{\mathbf{Q}}_{ce} = -(\mathbf{S}_{Qc} + \mathbf{\Omega}_c) \mathbf{Q}_{ce} - \mathbf{Q}_{crD}^2 \mathbf{S}_c \mathbf{R}_{cce} + \mathbf{E}_{Qc}^T \mathbf{H}_{ae} + \mathbf{S}_d \mathbf{H}_{de}, \\ (\mathbf{E}_{Qc} \mathbf{K}_c \mathbf{E}_{Qc}^T + \mathbf{K}_a) \mathbf{H}_{ae} = \mathbf{E}_{Qc} \mathbf{K}_c [(\mathbf{S}_{Qc} + \mathbf{\Omega}_c) \mathbf{Q}_{ce} + \mathbf{Q}_{crD}^2 \mathbf{S}_c \mathbf{R}_{cce} - \mathbf{S}_d \mathbf{H}_{de}] - \mathbf{K}_a \mathbf{\Omega}_a \mathbf{E}_{Qc} \mathbf{Q}_{ce} + \mathbf{Q}_{arD}^2 \mathbf{R}_{ae}, \end{cases} \quad (25)$$

where

$$\begin{aligned} \mathbf{\Omega}_c &= \text{diag}([\Omega_{c1}, \dots, \Omega_{cl}]) \\ \mathbf{\Omega}_a &= \text{diag}([\Omega_{a1}, \dots, \Omega_{a(n-l)}]) \\ \Omega_{ci} &= \begin{cases} R_{ci}(|Q_{ci}| + |Q_{cri}|), & Q_{ci} Q_{cri} \geq 0, \\ R_{ci} \frac{Q_{ci}^2 + Q_{cri}^2}{|Q_{ci}| + |Q_{cri}|}, & Q_{ci} Q_{cri} < 0, \end{cases} \\ \Omega_{ai} &= \begin{cases} R_{ai}(|Q_{ai}| + |Q_{ari}|), & Q_{ai} Q_{ari} \geq 0, \\ R_{ai} \frac{Q_{ai}^2 + Q_{ari}^2}{|Q_{ai}| + |Q_{ari}|}, & Q_{ai} Q_{ari} < 0, \end{cases} \end{aligned}$$

and matrices $\mathbf{\Omega}_c$ and $\mathbf{\Omega}_a$ are all positive-definite.

3.2. Globally Asymptotic Control Design

Choose the Lyapunov function as

$$V_1(\mathbf{Q}_{ce}) = \frac{1}{2} \mathbf{Q}_{ce}^T \mathbf{K}_c^{-1} \mathbf{Q}_{ce} \quad (26)$$

which represents the variation of kinetic energy stored in the FFN. Differentiate V_1 along the trajectory given by model (25),

$$\dot{V}_1(\mathbf{Q}_{ce}) = \mathbf{Q}_{ce}^T \mathbf{K}_c^{-1} \dot{\mathbf{Q}}_{ce} = -\mathbf{Q}_{ce}^T (\mathbf{\Omega}_c + \mathbf{S}_{Qc}) \mathbf{Q}_{ce} - \mathbf{Q}_{ce}^T \mathbf{Q}_{crD}^2 \mathbf{S}_c \mathbf{R}_{cce} + \mathbf{Q}_{ce}^T \mathbf{S}_d \mathbf{H}_{de} + \mathbf{Q}_{ce}^T \mathbf{E}_{Qc}^T \mathbf{H}_{ae} \quad (27)$$

Moreover, from the second equation of model (25),

$$\begin{aligned} \mathbf{H}_{ae}^T \mathbf{\Omega}_a^{-1} \mathbf{K}_a^{-1} (\mathbf{E}_{Qc} \mathbf{K}_c \mathbf{E}_{Qc}^T + \mathbf{K}_a) \mathbf{H}_{ae} &= \mathbf{H}_{ae}^T \mathbf{K}_a^{-1} \mathbf{\Omega}_a^{-1} \mathbf{E}_{Qc} \mathbf{K}_c [(\mathbf{S}_{Qc} + \mathbf{\Omega}_c) \mathbf{Q}_{ce} + \mathbf{Q}_{crD}^2 \mathbf{S}_c \mathbf{R}_{cce} - \mathbf{S}_d \mathbf{H}_{de}] \\ &\quad - \mathbf{H}_{ae}^T \mathbf{E}_{Qc} \mathbf{Q}_{ce} + \mathbf{H}_{ae}^T \mathbf{\Omega}_a^{-1} \mathbf{K}_a^{-1} \mathbf{Q}_{arD}^2 \mathbf{R}_{ae}, \end{aligned} \quad (28)$$

Through adding (27) and (28), we have

$$\begin{aligned} \dot{V}_1(Q_{ce}) = & -Q_{ce}^T(\Omega_c + S_{Qc})Q_{ce} - H_{ae}^T\Omega_a^{-1}K_a^{-1}(E_{Qc}K_cE_{Qc}^T + K_a)H_{ae} \\ & + H_{ae}^T\Omega_a^{-1}K_a^{-1}E_{Qc}K_c[(\Omega_c + S_{Qc})Q_{ce} + Q_{crD}^2S_cR_{cce} - S_dH_{de}] - Q_{ce}^TQ_{crD}^2S_cR_{cce} + \\ & Q_{ce}^TS_dH_{de} + H_{ae}^T\Omega_a^{-1}K_a^{-1}Q_{arD}^2R_{ae}. \end{aligned} \tag{29}$$

Design H_{de} , R_{cce} and R_{ae} as

$$H_{de} = -\Gamma_{cd}S_d^TQ_{ce} \tag{30}$$

$$R_{cce} = Q_{crD}^{-2}\Gamma_{cc}S_c^TQ_{ce} \tag{31}$$

$$R_{ae} = -Q_{arD}^{-2}\Gamma_aH_{ae} \tag{32}$$

respectively, where constant matrices Γ_d , Γ_{cc} and Γ_a are all positive-definite. Then, substitute (30)–(32) to (29),

$$\dot{V}_1(Q_{ce}) = -Q_{ce}^T(\Omega_c + S_{Qc} + \Gamma_c)Q_{ce} - H_{ae}^T\Pi_aH_{ae} + H_{ae}^T\Omega_a^{-1}K_a^{-1}E_{Qc}K_c(\Omega_c + S_{Qc} + \Gamma_c)Q_{ce} \tag{33}$$

where

$$\Gamma_c = S_{cd}\Gamma_{cd}S_{cd}^T + S_{cc}\Gamma_{cc}S_{cc}^T \tag{34}$$

$$\Pi_a = \frac{1}{2}\left\{\Omega_a^{-1}K_a^{-1}\left[E_{Qc}K_cE_{Qc}^T + K_a + \Gamma_a\right] + \left[E_{Qc}K_cE_{Qc}^T + K_a + \Gamma_a\right]K_a^{-1}\Omega_a^{-1}\right\}. \tag{35}$$

From Equation (33), if matrix inequality

$$K_a\Omega_a\Pi_a\Omega_aK_a \geq E_{Qc}K_c(\Omega_c + S_{Qc} + \Gamma_c)K_cE_{Qc}^T \tag{36}$$

is well satisfied, then

$$\dot{V}_e(Q_{ce}) \leq -\frac{1}{2}Q_{ce}^T(\Omega_c + S_{Qc} + \Gamma_c)Q_{ce} - \frac{1}{2}H_{ae}^T\Pi_aH_{ae} \tag{37}$$

i.e., the closed-loop is globally asymptotically stable. The above control design can be summarized as the following Proposition 2.

Proposition 2. Consider nonlinear differential-algebraic system (25) with the control input

$$H_d = H_{dr} - \Gamma_dS_d^TQ_{ce} \tag{38}$$

$$R_{cc} = R_{ccr} + Q_{crD}^{-2}\Gamma_{cc}S_c^TQ_{ce} \tag{39}$$

$$R_a = R_{ar} - Q_{arD}^{-2}\Gamma_aH_{ae} \tag{40}$$

Then, the closed-loop system globally asymptotically stable if matrix Inequality (36) is well satisfied.

Remark 2. Usually, due to the network parameter uncertainty, referenced vectors H_{dr} , R_{ccr} and R_{ar} are very hard to be obtained, which means that control laws (38)–(40) cannot be implemented in practical engineering. Therefore, it is necessary to design adaptive laws for the estimation of these parameters. Since H_{dr} , R_{ccr} and R_{ar} related to the practical feedwater headers and valve openings, it is reasonable to assume that they are norm-bounded, i.e.,

$$0 \leq H_{dr,i} \leq H_{drm}, \quad i = 1, \dots, m \tag{41}$$

$$0 \leq R_{ccr,i} \leq R_{ccrm}, \quad i = 1, \dots, l - m \tag{42}$$

$$0 \leq R_{ar,i} \leq R_{arm}, \quad i = 1, \dots, n - l \tag{43}$$

where H_{drm} , R_{ccrm} and R_{arm} are all given positive constants.

3.3. Adaptive Control Design

According to (38)–(40), choose the control input as

$$H_d = \hat{H}_{dr} - \Gamma_{cd} S_d^T Q_{ce} \tag{44}$$

$$R_{cc} = \hat{R}_{ccr} + Q_{crD}^{-2} \Gamma_{cc} S_c^T Q_{ce} \tag{45}$$

$$R_a = \hat{R}_{ar} - Q_{arD}^{-2} \Gamma_a H_{ae} \tag{46}$$

where \hat{H}_{dr} , \hat{R}_{ccr} and \hat{R}_{ar} are estimations of H_{dr} , R_{ccr} and R_{ar} respectively.

In order to design the adaptation laws for estimation \hat{H}_{dr} , \hat{R}_{ccr} and \hat{R}_{ar} , choose the extended LyaPunov function as

$$V_2(Q_{ce}, \tilde{H}, \tilde{R}_{ccr}, \tilde{R}_{ar}) = V_1(Q_{ce}) + \frac{1}{2} (\tilde{H}^T \Xi_d^{-1} \tilde{H} + \tilde{R}_{ccr}^T \Xi_{cc}^{-1} \tilde{R}_{ccr} + \tilde{R}_{ar}^T \Xi_a^{-1} \tilde{R}_{ar}) \tag{47}$$

where $\tilde{H} = \hat{H}_{dr} - H_{dr}$, $\tilde{R}_{ccr} = \hat{R}_{ccr} - R_{ccr}$, $\tilde{R}_{ar} = \hat{R}_{ar} - R_{ar}$ and constant diagonal matrices Ξ_d , Ξ_{cc} and Ξ_a are all positive-definite. Differentiate V_2 along the closed-loop trajectory given by model (25) and control inputs (44)–(46),

$$\begin{aligned} \dot{V}_2(Q_{ce}, \tilde{H}, \tilde{R}_{ccr}, \tilde{R}_{ar}) &= -Q_{ce}^T (\Omega_c + S_{Qc} + \Gamma_c) Q_{ce} - H_{ae}^T \Pi_a H_{ae} + H_{ae}^T \Omega_a^{-1} K_a^{-1} E_{Qc} K_c (\Omega_c + S_{Qc} + \Gamma_c) Q_{ce} \\ &\quad - Q_{ce}^T Q_{crD}^2 S_c \tilde{R}_{ccr} + Q_{ce}^T S_d \tilde{H} + H_{ae}^T \Omega_a^{-1} K_a^{-1} Q_{arD}^2 \tilde{R}_{are} + \tilde{H}^T \Xi_d^{-1} \dot{\hat{H}}_{dr} \\ &\quad + \tilde{R}_{ccr}^T \Xi_{cc}^{-1} \dot{\hat{R}}_{ccr} + \tilde{R}_{ar}^T \Xi_a^{-1} \dot{\hat{R}}_{ar} + H_{ae}^T \Omega_a^{-1} K_a^{-1} E_{Qc} K_c (Q_{crD}^2 S_c \tilde{R}_{ccr} - S_d \tilde{H}) \end{aligned} \tag{48}$$

Design the adaptation laws as

$$\dot{\hat{H}}_{dr} = \text{proj} \left(-\Xi_d S_d^T Q_{ce}, \quad H_{dr}, \quad m \right) \tag{49}$$

$$\dot{\hat{R}}_{ccr} = \text{proj} \left(\Xi_{cc} Q_{crD}^2 S_c^T Q_{ce}, \quad R_{ccr}, \quad l - m \right) \tag{50}$$

$$\dot{\hat{R}}_{ar} = \text{proj} \left(-\Xi_a Q_{arD}^2 K_a^{-1} \Omega_a^{-1} H_{ae}, \quad R_{ar}, \quad n - l \right) \tag{51}$$

where function $\text{proj}(\cdot)$ is defined by

$$\dot{\theta} = \text{proj} \left(\eta, \quad \theta_m, \quad k \right) = \left[\bar{\eta}_1 \quad \dots \quad \bar{\eta}_k \right]^T, \quad \theta, \eta \in \mathbb{R}^k \tag{52}$$

with scalar $\bar{\eta}_i$ given by

$$\bar{\eta}_i = \begin{cases} \eta_i & \theta_i = \theta_m, \eta_i < 0, \\ 0 & \theta_i = \theta_m, \eta_i > 0, \\ \eta_i & 0 < \theta_i < \theta_m, \\ 0 & \theta_i = 0, \eta_i < 0, \\ \eta_i & \theta_i = 0, \eta_i > 0, \end{cases} \quad i = 1, \dots, k. \tag{53}$$

From (41)–(43), (52) and (53), estimation \hat{H}_{dr} , \hat{R}_{ccr} and \hat{R}_{ar} as well as estimation error \tilde{H} , \tilde{R}_{ccr} and \tilde{R}_{ar} are all bounded.

Then, by substituting (49)–(51) to (48), if matrix inequality

$$K_a \Omega_a \Pi_a \Omega_a K_a \geq E_{Qc} K_c (\Omega_c + S_{Qc} + \Gamma_c + \Gamma_e) K_c E_{Qc}^T \tag{54}$$

is well satisfied, where Γ_e is an arbitrarily given positive-definite matrix and Π_a is given by Equation (35), then

$$\dot{V}_2 \leq -\frac{1}{2} Q_{ce}^T (\Omega_c + S_{Qc} + \Gamma_c) Q_{ce} - \frac{1}{2} H_{ae}^T \Pi_a H_{ae} + \left(Q_{crD}^2 S_c \tilde{R}_{ccr} - S_d \tilde{H} \right)^T \Gamma_e^{-1} \left(Q_{crD}^2 S_c \tilde{R}_{ccr} - S_d \tilde{H} \right) \tag{55}$$

which means that the closed-loop system is globally bounded stable.

The above adaptive control design can be summarized as the following Proposition 3.

Proposition 3. Consider nonlinear differential-algebraic system (25) with adaptive flowrate-pressure control given by

$$\begin{cases} \mathbf{H}_d = \hat{\mathbf{H}}_{dr} - \Gamma_d \mathbf{S}_d^T \mathbf{Q}_{ce}, \\ \mathbf{R}_{cc} = \hat{\mathbf{R}}_{ccr} + \mathbf{Q}_{crD}^{-2} \Gamma_{cc} \mathbf{S}_c^T \mathbf{Q}_{ce} \\ \mathbf{R}_a = \hat{\mathbf{R}}_{ar} - \mathbf{Q}_{arD}^{-2} \Gamma_a \mathbf{H}_{ae}, \\ \dot{\hat{\mathbf{H}}}_{dr} = \text{proj} \left(-\Xi_d \mathbf{S}_d^T \mathbf{Q}_{ce}, H_{drm}, m \right), \\ \dot{\hat{\mathbf{R}}}_{ccr} = \text{proj} \left(\Xi_{cc} \mathbf{Q}_{crD}^2 \mathbf{S}_c^T \mathbf{Q}_{ce}, R_{ccm}, l - m \right), \\ \dot{\hat{\mathbf{R}}}_{ar} = \text{proj} \left(-\Xi_a \mathbf{Q}_{arD}^2 \mathbf{K}_a^{-1} \Omega_a^{-1} \mathbf{H}_{ae}, R_{am}, n - l \right). \end{cases} \quad (56)$$

If Inequality (54) holds, then the closed-loop constituted by model (21) and adaptive control (56) is globally bounded stable.

Remark 3. From (56), the flowrate-pressure control law can be rewritten as

$$\begin{cases} \mathbf{H}_d = -\Gamma_d \mathbf{S}_d^T \mathbf{Q}_{ce} + \int_0^t \text{proj} \left(-\Xi_d \mathbf{S}_d^T \mathbf{Q}_{ce}, H_{drm}, m \right) ds, \\ \mathbf{R}_{cc} = \mathbf{Q}_{crD}^{-2} \Gamma_{cc} \mathbf{S}_c^T \mathbf{Q}_{ce} + \int_0^t \text{proj} \left(\Xi_{cc} \mathbf{Q}_{crD}^2 \mathbf{S}_c^T \mathbf{Q}_{ce}, R_{ccm}, l - m \right) ds, \\ \mathbf{R}_a = -\mathbf{Q}_{arD}^{-2} \Gamma_a \mathbf{H}_{ae} + \int_0^t \text{proj} \left(-\Xi_a \mathbf{Q}_{arD}^2 \mathbf{K}_a^{-1} \Omega_a^{-1} \mathbf{H}_{ae}, R_{am}, n - l \right) ds, \end{cases} \quad (57)$$

which takes form of proportional-integral (PI) feedback laws.

Remark 4. Moreover, the tuning method of FFN flowrate-pressure control law is determined from the design process given before Proposition 3. From inequality of (55) and (54) as well as Equation (35), the entries of diagonal positive-definite matrices Γ_d , Γ_c and Γ_a is larger, the speed of function V_2 converging to the origin is faster, which means that the errors of the flowrates and pressures decrease faster. Moreover, the function of positive matrices Ξ_d , Ξ_{cc} and Ξ_a is to make the steady control errors of flowrates and pressures to be zero.

Remark 5. The pressure-drop can be measured by the sensors such as elastic pressure gauge and membranometer, which depends on the scope of FFN operation pressure. The flowrate can be measured by difference pressure flow meter. Moreover, from Equation (57), flowrate-pressure control law are decentralized, which means that each flowrate or pressure control input only needs the measurement of the process variable regulated by this control input.

4. Application to a Nuclear-Solar Hybrid Plant

4.1. Feasibility of HES Based on MHTGR and STP

Due to the demand of clean renewable electric power, a number of CSP plant are being considered for deployment around the world. It has been pointed out by International Energy Agency (IEA) that CSP could provide 11.3% of global electricity by 2050. As introduced in Section 1, SPT plant is an important type of CSP plant and is also known as central receiver system. A SPT uses a heliostat field collector (HFC), i.e., a field of sun tracking reflectors called heliostat that reflect and concentrate the sunrays onto a central receiver placed in the top of a fixed tower. In the central receiver, heat is absorbed by a heat transfer fluid (HTF) such as the widely adopted molten salt, which then transfers heat to power a steam Rankine cycle. Relative to PTC, SPT achieves very high temperatures, which can increase the efficiency of conversion from heat to electricity and can also reduce the cost of thermal storage. Additionally, the piping system is concentrated in the central area of a SPT plant, which reduces the related energy losses, material costs and maintenance [31].

STPs with or without thermal storage are commonly equipped with a fuel backup system (BS) that helps to regulate production and to guarantee a nearly constant generation capacity. The integration of STP and BS modules can further reduce investments in reserving solar field and storage capacity [21,31]. Nowadays, the BS modules are usually realized through burning fossil fuels. Actually, since nuclear fission is a crucial clean base-load energy source that can substitute the fossil in a centralized way and in a great amount, it can be adopted for building the BS module of a STP, which induces the realization of nuclear-solar HESs with the virtue of persistent power supply. However, it is necessary to find the nuclear reactors with the ability of generating superheated steam, which can be coupled with STPs for building thermally coupled nuclear-solar HESs. Actually, modular high temperature gas-cooled reactor (MHTGR), which uses helium as the coolant and graphite as both the moderator and structure material, is a suitable fission reactor for building nuclear superheated steam supply system (Su-NSSS) modules that can be adopted as the BS of STP modules for realizing nuclear-solar hybrid plants.

The nuclear-solar HES composed of STP-based and MHTGR-based OTSSSs is a clean energy system fully free from carbon-emission. Due to its low power density, strong temperature negative feedback effect and large surface-to-volume ratio, MHTGR has the crucial inherent safety feature, which induces the simplification of safety-related systems and the reduction in reactor maintenance and leads to the feasibility of building MHTGR-STP coupled HES near large load centers. Moreover, since the primary coolant of MHTGR is helium and due to the high thermal efficiency of both MHTGR-based and SPT-based OTSSSs that induced by high live steam temperature, the water requirement of MHTGR-STP coupled HES should be lower than the pressurized water reactor (PWR) nuclear plant, PTC plant and their coupled HESs, which leads to the feasibility of building MHTGR-STP coupled HESs for the locations with water scarcity. Based on the above discussion, it can be seen that nuclear-solar HESs constituted by MHTGR-based and STP-based OTSSSs has the virtues of inherent nuclear safety, high thermal efficiency and low cost of construction and maintenance, which shows the strong feasibility of its deployment.

4.2. A MHTGR-STP Coupled HES

4.2.1. Schematic Diagram and Design Parameters

Figure 8 gives a schematic diagram of a nuclear-solar HES having two superheated steam supply system (4S) modules operating in parallel. Every 4S module is composed of a STP-based OTSSS and an MHTGR-based OTSSS and is independently equipped with a feedwater pump as well as a high-pressure heater (HPH). Moreover, for a 4S module, the feedwater is distributed to the MHTGR-based and STP-based OTSSSs of this module through adjusting the opening of governing valves. For the STP-based OTSSS, the molten salt is heated up in the central receiver to a high temperature by absorbing solar energy and transfers the heat to the feedwater for superheated steam production. For the MHTGR-based OTSSS, the cold helium is injected by the primary blower into the reactor core where it is heated up to a high temperature and flows to the primary-side of helical-coil OTSG where it turns the feedwater to superheated steam. The superheated live steam flows generated by the STP-based and MHTGR-based OTSSSs belonging to the two 4S modules are combined together to drive the turbine/generator set for electricity production. The condensed water is pressurized by the condensate pump and heated up by the low-pressure heater (LPH) successively and then flows into the deaerator. The water inside the common deaerator is fed to a 4S module by its feedwater pump and the feedwater is further heated up by the HPH before being distributed to the two OTSSSs in the same module for a new cycle. The designed values of the main parameters of MHTGR-based and STP-based OTSSSs at rated condition are given in Table 1 [13,32,33], where the main design parameters of the STP is computed based on [32,33].

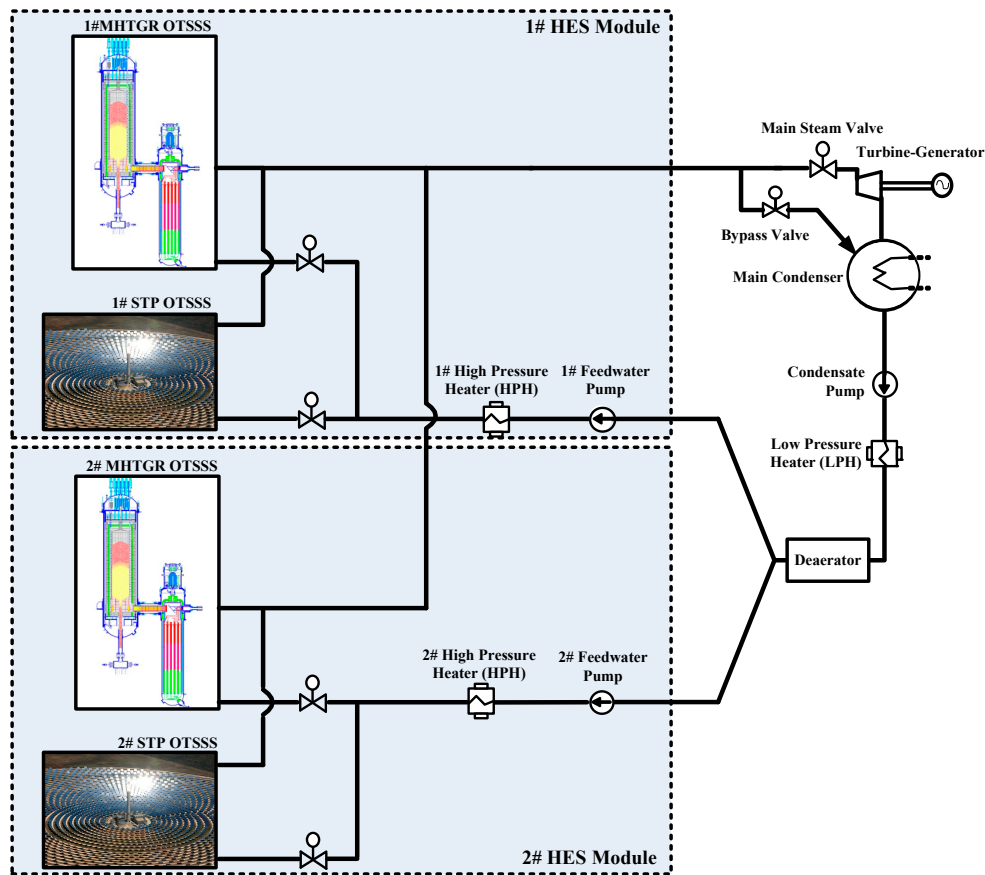


Figure 8. Schematic diagram of a nuclear-solar multimodular hybrid energy system (HES).

Table 1. Main design parameters of the nuclear-solar hybrid energy system (HES) at rated condition.

	Parameter	Unit	Value
Plant	Maximal Plant thermal power	MW _t	800
	Maximal Plant electrical power	MW _e	320
	Number of modules		2
	Main steam temperature	°C	571
	Main steam pressure	MPa	13.9
MHTGR-Based OTSS	Rated thermal power	MW _{th}	250
	Average core power density	MW/m ³	3.22
	Active core diameter/height	m	3/11
	Primary helium pressure	MPa	7
	Helium temperature at reactor inlet/outlet	°C	277/750
	Helium flowrate	kg/s	102
	Feedwater temperature	°C	250
Feedwater flowrate	kg/s	103	
STP-Based OTSS	Rated thermal power	MW _{th}	150
	Heat transfer fluid (HTF)		Molten nitrate salt mixture (60 wt % NaNO ₃ , 40 wt % KNO ₃)
	HTF temperature at cold/hot leg	°C	432/700
	HTF flowrate	kg/s	368
	Feedwater temperature	°C	250
Feedwater flowrate	kg/s	61	

4.2.2. Secondary FFN and Control Strategy

Moreover, the secondary FFN of this two-modular nuclear-solar HES is shown in Figure 9, where branches f1 and f2 are the pump branches including the feedwater pump and high pressure heater (HPH), branch $2i - 1$ is the secondary side of the i th MHTGR-based OTSSS ($i = 1, 2$), branch $2i$ is the secondary side of the i th STP-based OTSSS ($i = 1, 2$) and branch 5 composes of the equipment such as the turbine, condenser, low pressure heater (LPH) and deaerator. Since the realization and stable operation of the two-modular nuclear-solar HES shown in Figure 9 heavily depends on the condition that the pressure of the live steam flows generated by different OTSSSs of the two modules should be identical in both steady and transient states, it is necessary to regulate the OTSSS flowrates and main steam pressure, which are just the flowrates of branch i ($i = 1, \dots, 4$) and pressure-drops of branch 5 of the secondary FFN shown in Figure 9 respectively. Here, the newly-built adaptive flowrate-pressure control law (57) is applied to solve this FFN regulation problem, where header H_d adjusted by the rotation speed of pumps is utilized to regulate the flowrates of branches 1 and 2, resistance R_{cc} adjusted by the opening of feedwater valves in branches 3 and 4 is utilized to regulate the corresponding flowrates and resistance R_a adjusted by the steam valve opening is utilized to regulate the main steam pressure.

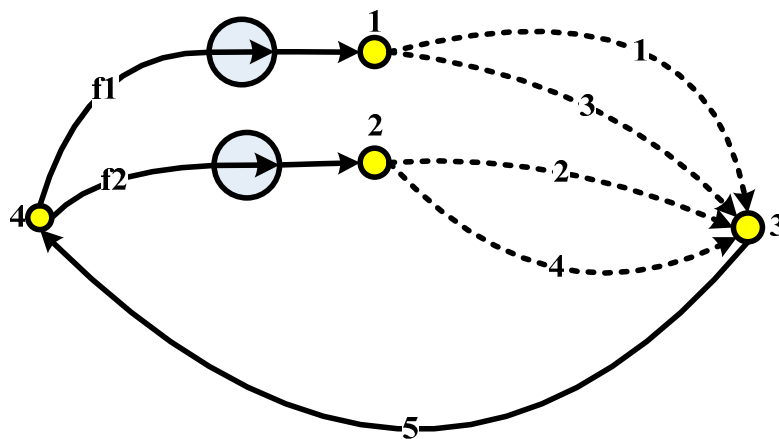


Figure 9. FFN of the nuclear-solar hybrid energy system (HES).

4.3. Simulation Results with Discussions

4.3.1. Controller Parameters

For the FFN given by Figure 9, it can be seen that $n_c = 4$, $m = 2$, $n = 5$, $l = 4$ and topology matrices E_{Qc} and e_{Qfc} are given by

$$E_{Qc} = \begin{bmatrix} -1 & -1 & -1 & -1 \end{bmatrix}$$

$$e_{Qfc} = \begin{bmatrix} 1 & 0 & 1 & 0 \\ 0 & 1 & 0 & 1 \end{bmatrix}$$

respectively. In this simulation, the network parameters are chosen to be $K_i = 0.1$ (kg/MPa·s²) ($i = 1, \dots, 5$), $R_1 = R_2 = 0.006$ MPa/(kg/s)², $R_{f1} = R_{f2} = 0.0001$ MPa/(kg/s)² and the parameters FFN pressure-flowrate controller (56) are set to be $\Gamma_d = 0.5I_2$, $\Pi_d = 100I_2$, $\hat{H}_{dr0} = O$, $\Gamma_{cc} = 0.05 Q_{crD}^2$, $\Pi_{cc} = 200 Q_{crD}^2$, $\hat{R}_{ccr0} = O$, $\Gamma_a = 0.01 Q_{arD}^2$, $\Pi_a = 1 \times 10^3 Q_{arD}^2$ and $\hat{R}_{ar,0} = 0$. The MHTGR-based OTSSS control adopts the one given in [34]. For the STP-based OTSSS, molten salt flowrate is utilized to regulate the receiver outlet temperature and feedwater flowrate is applied for regulating the live steam temperature, where PI algorithms are adopted [35,36]. The case study of the ramp switch from

the nuclear to solar power and its inverse are studied in this numerical simulation which was done in Matlab/Simulink.

4.3.2. Simulation Cases and Results

Initially, both 1# and 2# MHTGRs operate at 250 MW_{th} and 1# and 2# STPs run at 30 MW_{th} and 50 MW_{th} respectively, which corresponds to the case of cloudy or nighttime period. Then, at 20,000 s, 1# and 2# MHTGRs maneuver from 250 MW_{th} to 150 MW_{th} and 125 MW_{th} respectively with a constant speed of 12.5 MW_{th}/min and at the same time, 1# and 2# STPs maneuver respectively from 30 MW_{th} and 50 MW_{th} to 150 MW_{th} with a constant speed of 7.5 MW_{th}/min, which corresponds to the switch from nuclear power to solar power. Furthermore, at 40,000 s, 1# and 2# MHTGRs start to maneuver back to 250 MW_{th} with a constant speed of 12.5 MW_{th}/min and 1# and 2# STPs maneuver back to the power-level of 30 MW_{th} and 50 MW_{th} respectively in a speed of 7.5 MW_{th}/min.

The responses of 1# MHTGR-based OTSSS, i.e., the normalized nuclear power, reactor outlet helium temperature, live steam temperature, primary helium flowrate and secondary feedwater flowrate are shown in Figure 10 and the responses of 2# MHTGR-based OTSSS are shown in Figure 11. The responses of 1# SPT-based OTSSS, i.e., the outlet and inlet molten salt of the receiver, live steam temperature, flowrates of molten salt and feedwater are shown in Figure 12 and the responses of 2# SPT-based OTSSS are given in Figure 13. The responses of main steam pressure, header given by 1# and 2# feedwater pump and fluid resistance caused by governing valves in branch 3 and 4 are all given in Figure 14. The responses thermal power of different OTSSSs and HES modules are shown in Figure 15.

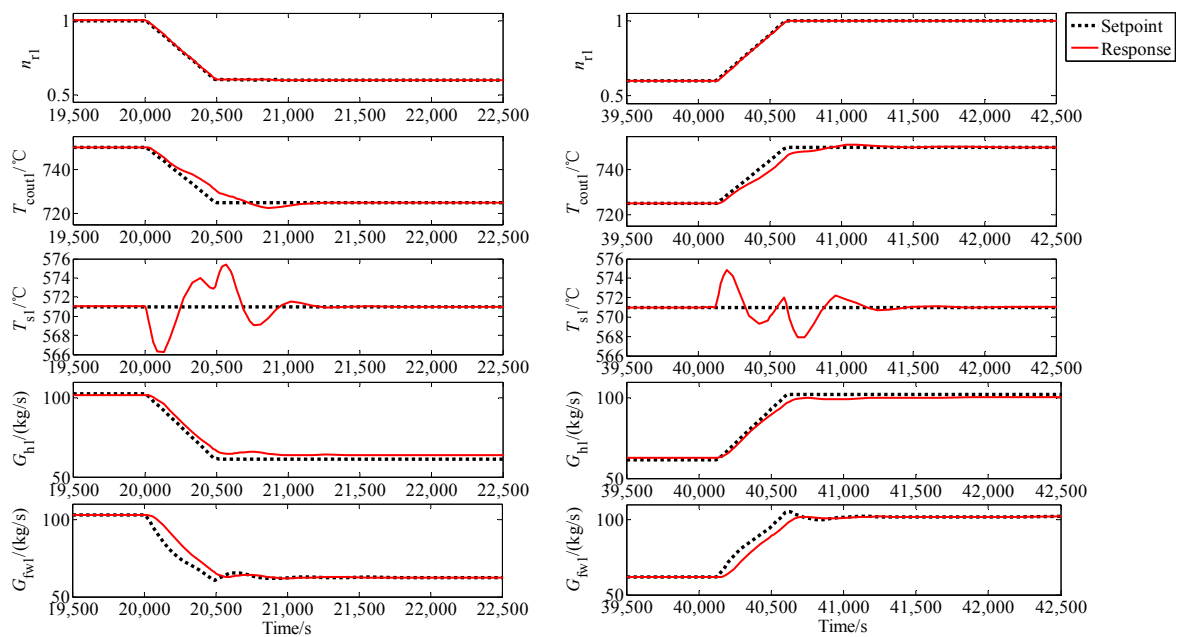


Figure 10. Responses of 1# MHTGR-based OTSSS, n_{r1} : normalized nuclear power, T_{cout1} : reactor outlet helium temperature, T_{s1} : live steam temperature, G_{h1} : primary helium flowrate, G_{fw1} : secondary feedwater flowrate.

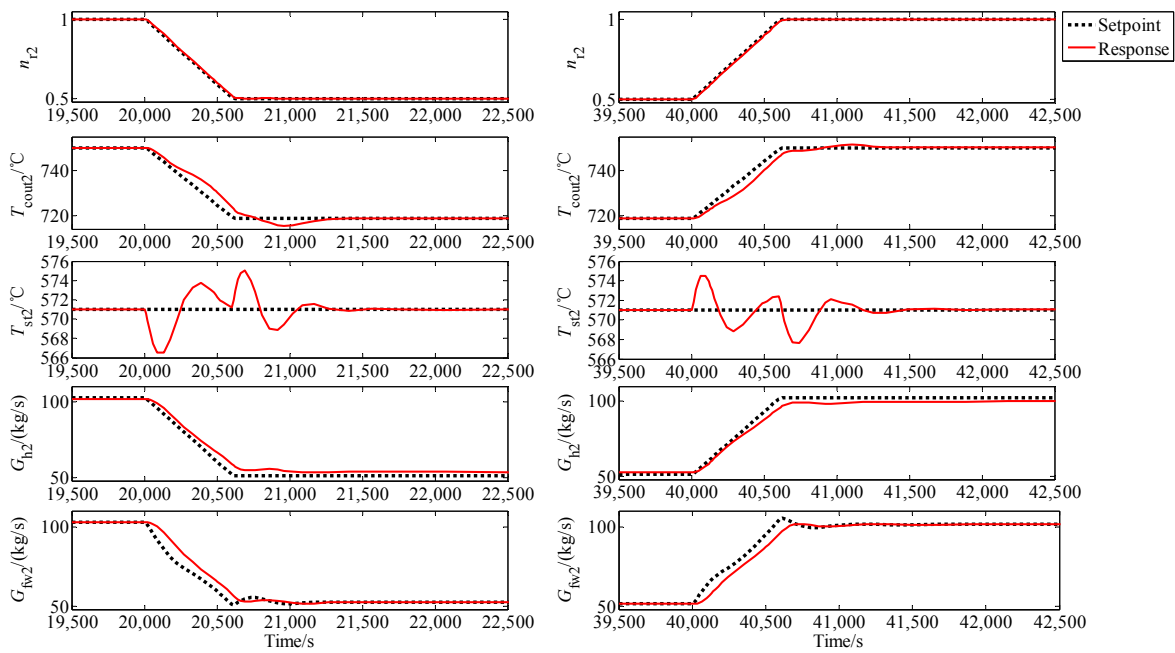


Figure 11. Responses of 2# MHTGR-based OTSS, n_{r2} : normalized nuclear power, T_{cout2} : reactor outlet helium temperature, T_{st2} : live steam temperature, G_{h2} : primary helium flowrate, G_{fw2} : secondary feedwater flowrate.

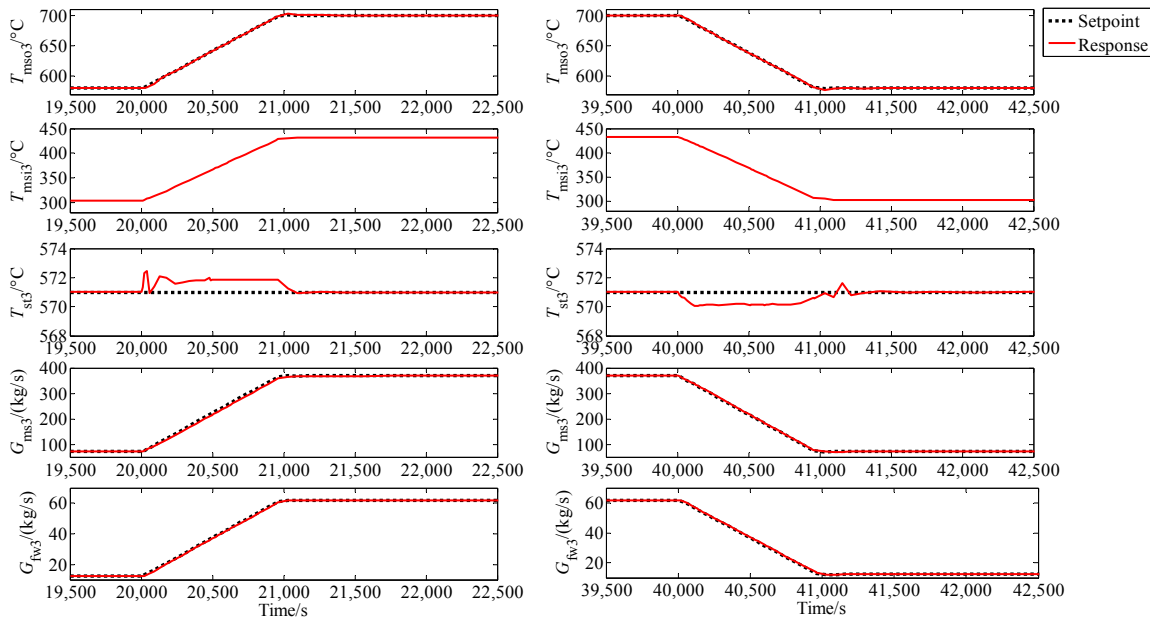


Figure 12. Responses of 1# STP-based OTSS, T_{mso3} : receiver outlet molten salt temperature, T_{msi3} : receiver inlet molten salt temperature, T_{st3} : live steam temperature, G_{ms1} : primary molton salt flowrate, G_{fw1} : secondary feedwater flowrate.

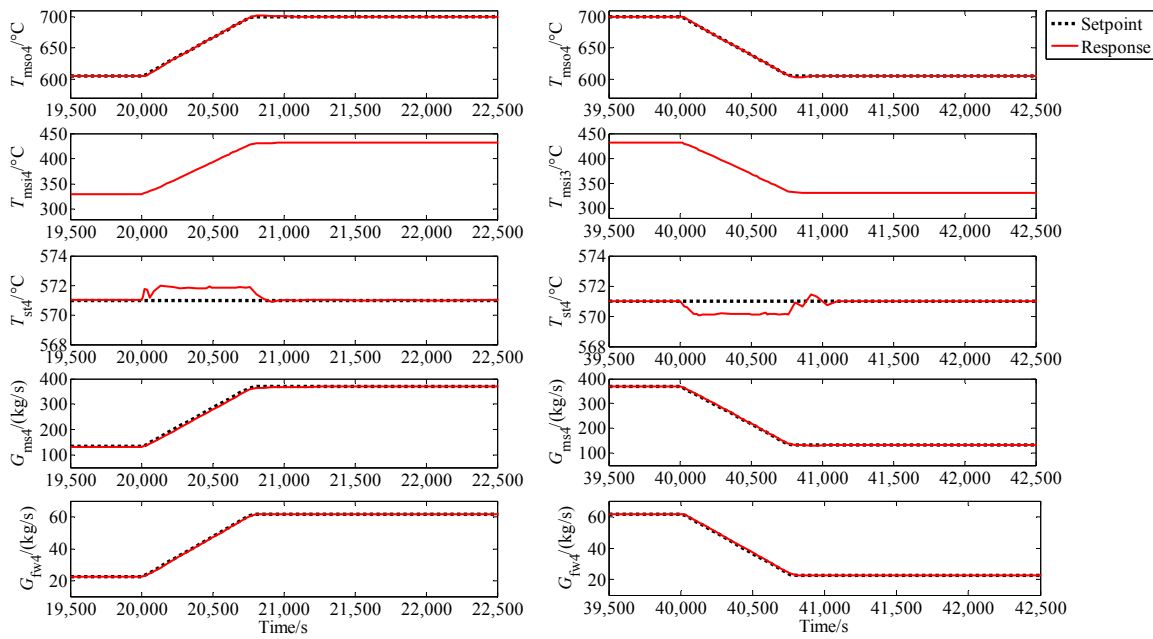


Figure 13. Responses of 2# STP-based OTSSS, T_{ms04} : receiver outlet molten salt temperature, T_{ms14} : receiver inlet molten salt temperature, T_{st4} : live steam temperature, G_{ms4} : primary molton salt flowrate, G_{fw4} : secondary feedwater flowrate.

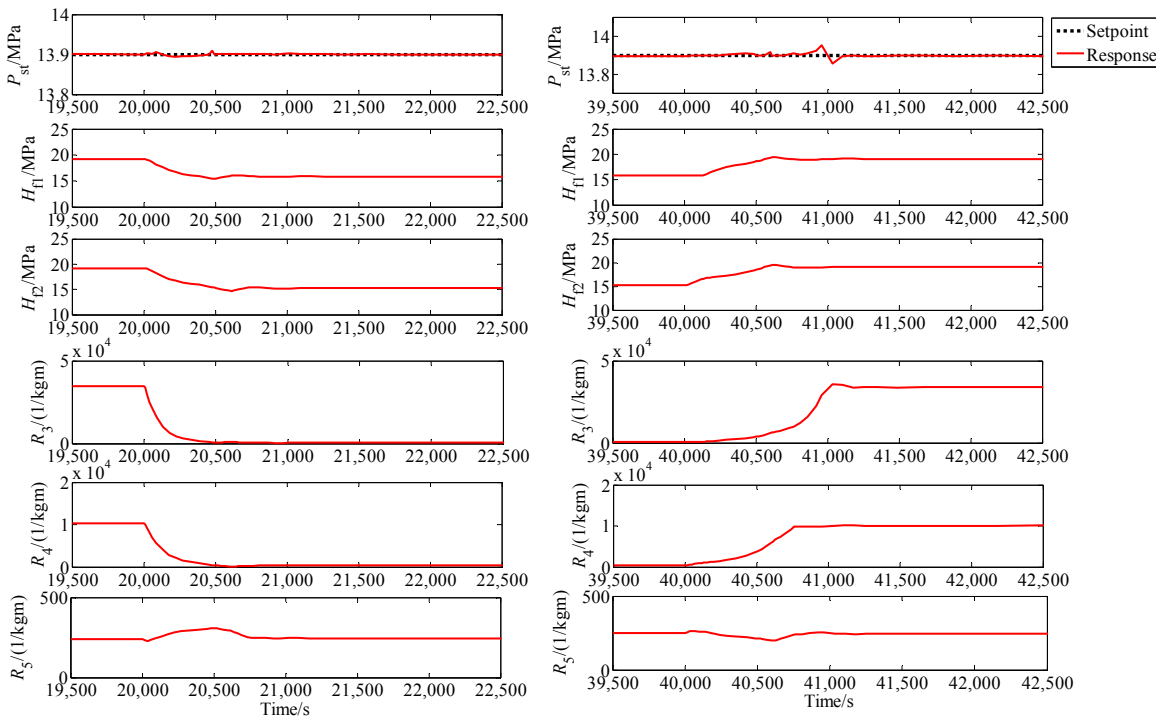


Figure 14. Responses of main steam pressure, feedwater header and branch resistances, P_{st} : main steam pressure, H_{f1} and H_{f2} : header given by 1# and 2# feedwater pump, R_i : fluid resistances in branch i ($i = 3, 4, 5$).

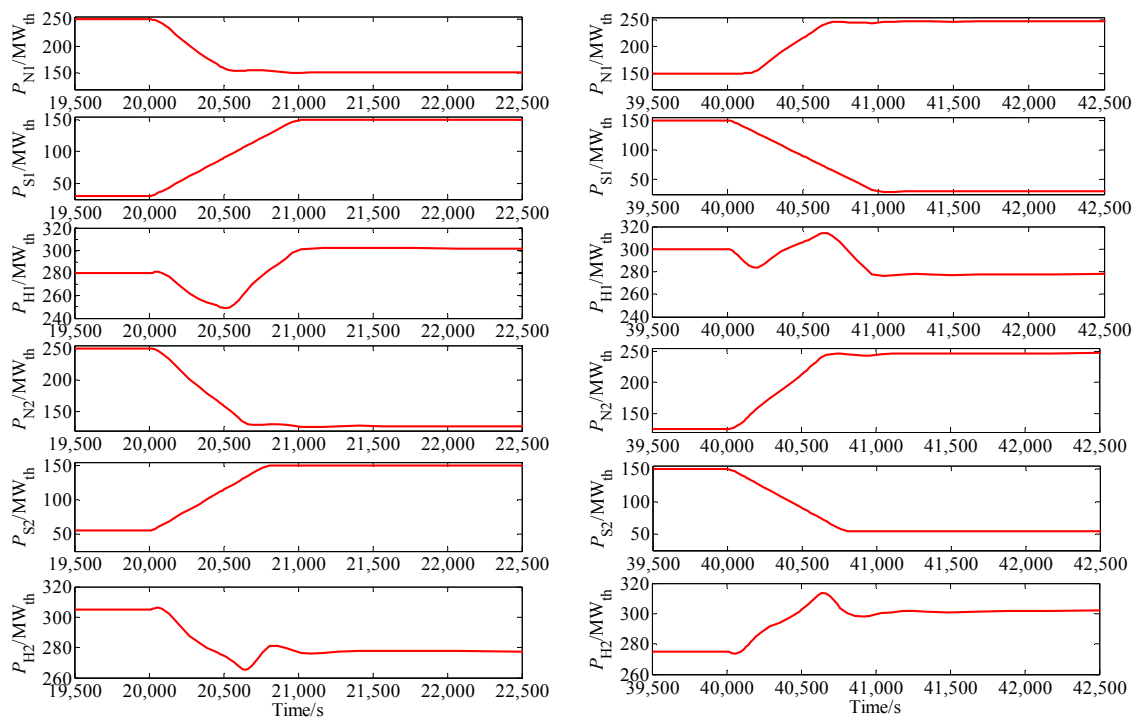


Figure 15. Responses of thermal powers, P_{Ni} : thermal power of i # MHTGR-based OTSSS, P_{Si} : thermal power of i # STP-based OTSSS, P_{Hi} thermal power of i # HES module composed of i # MHTGR-based OTSSS and i # STP-based OTSSS ($i = 1, 2$).

4.3.3. Discussions

The transience happens at 20,000 s is just a switch from nuclear power to solar power. From the left column of Figures 10, 11 and 15, it can be seen that 1# and 2# MHTGR-based OTSSSs maneuver stably from the power-level of 250 MW_{th} to that of 150 and 125 MW_{th} respectively. From the left column of Figures 12, 13 and 15, it can also be seen that the power-levels of 1# and 2# STP-based OTSSS increase smoothly from 30 and 50 to 150 MW_{th} respectively. This power-level maneuver of different OTSSSs relies not only on the control laws of MHTGR-based and STP-based OTSSSs but also heavily on the pressure-flowrate control of secondary FFN with topological structure shown in Figure 9. Since the pump headers is utilized to control the feedwater flowrates of the MHTGR-based OTSSSs, the headers should be reduced in the case of MHTGR power-level decrease. However, the power increase of STP-based OTSSSs needs the increase of feedwater header, which is in contradict with the reduction of pump headers but can be realized by enlarging the opening of the governing valves located in branch 3 and 4. The variation of the OTSSS flowrates can further induce the fluctuation of main steam pressure, which can be suppressed by the steam valve mounted in branch 5. From the left column of Figure 14, FFN control law (57) can guarantee satisfactory transience for branch flowrates and stability for main steam pressure.

Similarly, the transience starts at 40,000 s is a switch from solar power to nuclear power, which may be happens in cloudy days or nighttime. The MHTGR power-level increase needs the increase in pump headers that are adopted to regulate the feedwater flowrates of MHTGR-based OTSSSs, which can also lead to the increase of the feedwater flowrates of STP-based OTSSSs. To realize decrease the feedwater flowrates of STP-based OTSSSs, which is necessary for power-level reduction, the opening of the governing valves in branches 3 and 4 should be lessen. The steam pressure should also be well maintained during the switch from solar power to nuclear power. As we can see from the right column of Figure 14, due to the feedback effect of FFN controller (57), the responses of branch flowrates and steam pressures are satisfactory. Moreover, from the right column of Figures 10–13 and 15, 1# and

2# MHTGR-based OTSSs maneuver stably from 150 and 125 MW_{th} back to 250 MW_{th} respectively and the thermal powers 1# and 2# STP-based OTSSs also smoothly decrease to 30 and 50 MW_{th} from 150 MW_{th}.

In a summary, the FFN control law (57) realizes the coordinated control of the two HES modules, constituted by a STP-based OTSSS and an MHTGR-based OTSSS, which plays a key role in building thermally coupled multimodular and hybrid energy systems. From (57), this newly-built FFN controller is just composed of some simple decentralized PI feedback laws with knowledge of plant physical and thermal-hydraulic parameters which are easy to be implemented and commissioned on current digital control system platforms.

5. Conclusions

Multimodular and hybrid energy systems can be built by integrating multiple homogeneous or heterogeneous OTHSS modules based on renewable, nuclear or fossil energy sources, where the module integration can be realized through FFNs. Thus, modeling and flowrate-pressure control of FFNs is crucial for those multimodular and hybrid energy systems with modules interconnected by FFNs. In the aspect of dynamical modeling, a simple control-design-oriented nonlinear differential-algebraic model for the FFNs with multiple pump branches is first proposed based on branch dynamics and network graph property. In the aspect of control design, a novel adaptive decentralized flowrate-pressure control law is given for FFNs with multiple pumps, which can provide satisfactory closed-loop stability as well as transient performance and does not need the values of plant physical and thermal-hydraulic parameters. Moreover, this newly-built FFN controller takes a proportional-integral (PI) form with saturation in the integration term, which induces easy practical implementation. Finally, this new controller has been applied to the power-level maneuver of a two-modular nuclear-solar HES constituted by MHTGR-based and STP-based OTSSs and realize the regulation of feedwater flowrates of different OTSSs and stabilization of main steam pressure. Simulation results show the feasibility and high performance of this new FFN controller. The novelty of this paper focuses on converting the control of hybrid and multimodular energy system to modeling and flowrate-pressure control design for FFNs. One of the future research work is to apply the results in this paper to the control of other types of HESs driven by the fossil, nuclear and renewables.

Acknowledgments: This work is jointly supported by the National S&T Major Project of China (Grant Nos. 2008ZX06901, 2010ZX06906) and the Natural Science Foundation of China (NSFC) (Grant No. 61374045, 61773228).

Author Contributions: Zhe Dong gave the modeling and the pressure-flowrate control law for fluid flow networks. Yifei Pan developed the simulation software, and did the verification. Zuoyi Zhang, Yujie Dong and Xiaojin Huang led this research work. Zuoyi Zhang provides the design result of the MHTGR-based NSSS. Yujie Dong gives the design result for the secondary-circuit of the plant. Xiaojin Huang develops the operation strategy for the hybrid plant.

Conflicts of Interest: The authors declare no conflict of interest.

References

1. Ruth, M.F.; Zinaman, O.R.; Antkowiak, M.; Boardman, R.D.; Cherry, R.S.; Bazilian, M.D. Nuclear-renewable hybrid energy systems: Opportunities, interconnections and needs. *Energy Convers. Manag.* **2014**, *78*, 684–694. [[CrossRef](#)]
2. Montes, M.J.; Rovira, A.; Muñoz, M.; Martínez-Val, J.M. Performance analysis of an integrated solar combined cycle using direct steam generation in parabolic through collectors. *Appl. Energy* **2011**, *88*, 3228–3238. [[CrossRef](#)]
3. Ingersoll, D.T. Deliberately small reactors and the second nuclear era. *Prog. Nucl. Energy* **2009**, *51*, 589–603. [[CrossRef](#)]
4. Vujčić, J.; Bergmann, R.M.; Škoda, R.; Miletić, M. Small modular reactors: Simpler, safer, cheaper? *Energy* **2012**, *45*, 288–295. [[CrossRef](#)]

5. Rowinski, M.K.; White, T.J.; Zhao, J. Small and medium sized reactors (SMR): A review of technology. *Renew. Sustain. Energy Rev.* **2015**, *44*, 643–656. [[CrossRef](#)]
6. Ingersoll, D.T.; Houghton, Z.J.; Bromm, R.; Desportes, C. Nuscale small modular reactor for co-generation of electricity and water. *Desalination* **2014**, *340*, 84–93. [[CrossRef](#)]
7. Reutler, H.; Lohnert, G.H. The modular high-temperature reactor. *Nucl. Technol.* **1983**, *62*, 22–30. [[CrossRef](#)]
8. Reutler, H.; Lohnert, G.H. Advantages of going modular. *Nucl. Eng. Des.* **1984**, *78*, 129–136. [[CrossRef](#)]
9. Lohnert, G.H. Technical design features and essential safety-related properties of the HTR-MODULE. *Nucl. Eng. Des.* **1990**, *121*, 259–275. [[CrossRef](#)]
10. Lanning, D.D. Modularized high-temperature gas-cooled reactor systems. *Nucl. Technol.* **1989**, *88*, 139–156. [[CrossRef](#)]
11. Zhang, Z.; Sun, Y. Economic potential of modular reactor nuclear power plants based on the Chinese HTR-PM project. *Nucl. Eng. Des.* **2007**, *237*, 2265–2274. [[CrossRef](#)]
12. Zhang, Z.; Wu, Z.; Wang, D.; Xu, Y.; Sun, Y.; Li, F.; Dong, Y. Current status and technical description of Chinese 2 × 250 MWth HTR-PM demonstration plant. *Nucl. Eng. Des.* **2009**, *239*, 1212–1219. [[CrossRef](#)]
13. Zhang, Z.; Dong, Y.; Li, F.; Zhang, Z.; Wang, H.; Huang, X.; Li, H.; Liu, B.; Wu, X.; Wang, H.; et al. The shandong shidao bay 200 MW_e high-temperature-gas-cooled reactor pebble-bed module (HTR-PM) demonstration power plant: An engineering and technological innovation. *Engineering* **2016**, *2*, 112–118. [[CrossRef](#)]
14. Flueckiger, S.M.; Iverson, B.D.; Garimella, S.V.; Pacheco, J.E. System-level simulation of a solar power tower plant with thermocline thermal energy storage. *Appl. Energy* **2014**, *113*, 86–96. [[CrossRef](#)]
15. Peng, S.; Hong, H.; Wang, Y.; Wang, Z.; Jin, H. Off-design thermodynamic performances on typical days of a 330 MW solar aided coal-fired power plant in China. *Appl. Energy* **2014**, *130*, 500–509. [[CrossRef](#)]
16. Kim, K.K.; Bernard, J.A. Considerations in the control of PWR-type multimodular reactor plants. *IEEE Trans. Nucl. Sci.* **1994**, *41*, 2686–2697.
17. Garcia, H.E.; Chen, J.; Kim, J.S.; Vilim, R.B.; Binder, W.R.; Sitton, S.M.B.; Boardman, R.D.; McKellar, M.G.; Paredis, C.J.J. Dynamic performance analysis of two regional nuclear hybrid energy systems. *Energy* **2016**, *107*, 234–258. [[CrossRef](#)]
18. Lykidi, M.; Gourdel, P. How to manage flexible nuclear power plants in a deregulated electricity market from the point of view of social welfare? *Energy* **2015**, *85*, 167–180. [[CrossRef](#)]
19. Perillo, S.R.P.; Upadhyaya, B.R.; Li, F. Control and instrumentation strategies for multi-modular integral nuclear reactor systems. *IEEE Trans. Nucl. Sci.* **2011**, *58*, 2442–2451. [[CrossRef](#)]
20. Dong, Z.; Song, M.; Huang, X.; Zhang, Z.; Wu, Z. Module coordination control of MHTGR-based multi-modular nuclear plants. *IEEE Trans. Nucl. Sci.* **2016**, *63*, 1889–1900. [[CrossRef](#)]
21. Zhang, H.L.; Baeyens, J.; Degreève, J.; Cacères, G. Concentrated solar power plants: Review and design methodology. *Renew. Sustain. Energy Rev.* **2013**, *22*, 466–481. [[CrossRef](#)]
22. Mahdi, A.A.; McPherson, M.J. An introduction to automatic control of mine ventilation systems. *Min. Technol.* **1971**, *53*, 5–10.
23. DeMoyer, R.J. System modeling and simulation for water distribution control. *Model. Simul.* **1974**, *5*, 185.
24. Rao, H.S. Modeling of water distribution systems. In Proceedings of the 16th IEEE Conference on Decision and Control, New York, NY, USA, 7–9 December 1977; pp. 653–658.
25. Kocić, D.D. On the autonomy of local systems in ventilation control. In Proceedings of the 2nd Mine Ventilation Congress, Reno, NV, USA, 4–8 November 1979.
26. Hu, Y.; Koroleva, O.I.; Kristić, M. Nonlinear control of mine ventilation networks. *Syst. Control Lett.* **2003**, *49*, 239–254. [[CrossRef](#)]
27. Dong, Z. Dissipation analysis and adaptive control of fluid networks. In Proceedings of the American Control Conference, Chicago, IL, USA, 1–3 July 2015; pp. 671–676.
28. Dong, Z.; Song, M.; Huang, X.; Zhang, Z.; Wu, Z. Coordination control of SMR-based NSSS modules integrated by feedwater distribution. *IEEE Trans. Nucl. Sci.* **2016**, *63*, 2682–2690. [[CrossRef](#)]
29. Ward-Smith, A.J. *Internal Fluid Flow—The Fluid Dynamics of Flow in Pipes and Ducts*; Clarendon Press: Oxford, UK, 1980.
30. Desoer, C.A.; Kuh, E.S. *Basic Circuit Theory*; McGraw-Hill: New York, NY, USA, 1969.
31. Reddy, V.S.; Kaushik, S.C.; Ranjan, K.R.; Tyagi, S.K. State-of-the-art of solar thermal power plants—A review. *Renew. Sustain. Energy Rev.* **2013**, *27*, 258–273. [[CrossRef](#)]

32. Li, X.; Kong, W.; Wang, Z.; Chang, C.; Bai, F. Thermal model and thermodynamic performance of molten salt cavity receiver. *Renew. Energy* **2010**, *35*, 981–988. [[CrossRef](#)]
33. Benammar, S.; Khellaf, A.; Mohammedi, K. Contribution to the modeling and simulation of solar power tower plants using energy analysis. *Energy Convers. Manag.* **2014**, *78*, 923–930. [[CrossRef](#)]
34. Dong, Z.; Pan, Y.; Zhang, Z.; Dong, Y.; Huang, X. Model-free adaptive control law for nuclear superheated-steam supply systems. *Energy* **2017**, *135*, 53–67. [[CrossRef](#)]
35. Camacho, E.F.; Rubio, F.R.; Berenguel, M.; Valenzuela, L. A survey on control schemes for distributed solar collector fields. Part I: Modeling and basic control approaches. *Sol. Energy* **2007**, *81*, 1240–1251. [[CrossRef](#)]
36. Cirre, C.M.; Berenguel, M.; Valenzuela, L.; Camacho, E.F. Feedback linearization control for a distributed solar collector field. *Control Eng. Pract.* **2007**, *15*, 1533–1544. [[CrossRef](#)]



© 2017 by the authors. Licensee MDPI, Basel, Switzerland. This article is an open access article distributed under the terms and conditions of the Creative Commons Attribution (CC BY) license (<http://creativecommons.org/licenses/by/4.0/>).